CHEMISTRY OF MATERIALS

ACS Editors' Choice

Article

pubs.acs.org/cm

Selectively Controlled Orientational Order in Linear-Shaped Thermally Activated Delayed Fluorescent Dopants

Takeshi Komino,[†,‡] Hiroyuki Tanaka,[‡] and Chihaya Adachi*[,†,‡,§]

[†]Education Center for Global Leaders in Molecular System for Devices, [‡]Center for Organic Photonics and Electronics Research (OPERA), and [§]International Institute for Carbon Neutral Energy Research (WPI-I2CNER), Kyushu University, 744 Motooka, Nishi, Fukuoka 819-0395, Japan

Supporting Information

ABSTRACT: The orientational order of a linear-shaped thermally activated delayed fluorescent dopant 10-[4-(4,6-diphenyl-1,3,5-triazin-2-yl)phenyl]-10*H*-phenoxazine (PXZ-TRZ) was selectively controlled in a randomly oriented host matrix composed of 3,3-di(9*H*-carbazol-9-yl)biphenyl (mCBP) by varying the temperature during deposition of the thin films. Although the molecular orientation of mCBP was random at deposition temperatures ranging from 200 to 300 K (orientational disorder), PXZ-TRZ molecules oriented horizontal to the substrate in this temperature range (high orientational order). This indicates that the orientational order was dominated by the kinetic behavior of PXZ-TRZ at the film surface rather than by randomization caused by aggregation of PXZ-TRZ and mCBP molecules. Using an orientation-controlled 6 wt % PXZ-TRZ:mCBP film as an emitting layer, we fabricated organic light-emitting diodes (OLEDs). The horizontal orientation of the dopants enhanced the external electroluminescence quantum efficiency of the OLED by 24% compared with that of the corresponding OLED with slightly vertical orientation. An optical simulation found that the enhancement originates mainly from the improvement of the light out-coupling efficiency.

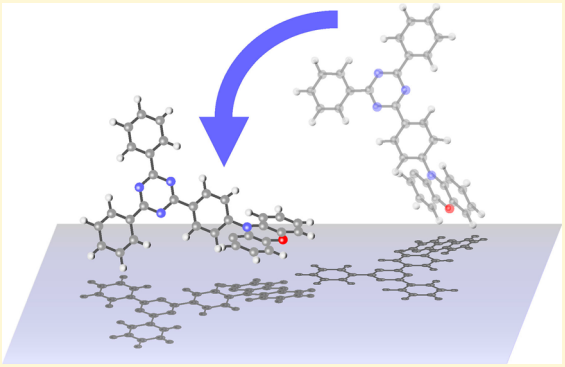

INTRODUCTION

A special feature of a thin film surface is that it markedly influences successive film growth during deposition. Various deposition conditions affect the molecular and/or atomic configurations and their dynamics at surfaces, and indirectly define the resulting configurations of entire films. Temperature control is generally used to tune deposition conditions because molecular and atomic dynamics are influenced by internal energy. For example, well-defined crystals can be formed under suitable conditions by adjusting the deposition temperature ($T_{deposition}$) during epitaxial crystal growth.[1] Methodology using temperature control is effective to determine molecular configurations not only in systems with long-range order but also in disordered systems consisting of small molecules. Recently, Ediger and co-workers reported that indomethacin glass formed by vapor deposition is one of three types depending on distinct $T_{deposition}$ regimes: equilibrium, quasi-equilibrium, and kinetically controlled.[2] The kinetically controlled regime, which is the lowest temperature regime and much lower than the glass transition temperature (T_g), generates anisotropic dipole orientations as a result of the slower rate of molecular configurational sampling at the film surface than deposition rate, so the dynamic behavior of the molecules on the surface is kinetically controlled. To date, Lin et al.,[3−5] Yokoyama et al.,[6−12] our group,[9−17] and others[12,18−23] have reported a large number of organic noncrystalline films showing preferential orientations. These experimental results led us to consider that anisotropic materials could possibly be categorized as glasses formed under kinetically controlled regimes. Our previous studies have regarded the threshold temperature to produce kinetically controlled and isotropic ordinary glasses as T_g at the surface through analogy with that in the field of polymers.[24−26] This is because the distinctive feature of this temperature is very similar to that in polymers,[27−30] i.e., T_g at the surface is much lower than bulk T_g. In fact, thickness-dependent elastic moduli, which are analogous to the behavior of thin polymer films being influenced by free surface effects, were also reported for thin films of small molecules frequently used in organic light-emitting diodes (OLEDs).[31,32] We express this temperature as T_g(surface) hereafter.

The kinetically controlled regime below T_g(surface) is of potential interest in molecular science because it can homogeneously and continuously control orientational order over a wide range, thus determining the optical and electric properties of organic thin films. For example, preferential orientations have been revealed to affect the probabilities of charge transfer (CT) at metal/organic[15] and organic/

Received: March 6, 2014
Revised: May 26, 2014
Published: May 26, 2014

   dx.doi.org/10.1021/cm500802p | Chem. Mater. 2014, 26, 3665−3671

organic[33,34] interfaces, charge carrier mobilities,[7,9,10,14,15,25,26] densities of states,[25] and light propagation.[4,5,13,16] In addition, the wide variety of the dependence of optoelectronic characteristics on molecular orientation should allow us to further advance organic devices, because such dependence means we can greatly expand their advantages compared with other competing inorganic devices with optical and electronic anisotropy from which an anisotropic molecular shape originates. In particular, linear-shaped molecules have been revealed to form highly oriented films with an orientational order parameter of $S < -0.45$,[12,13,26] so they are promising compounds for investigating the effects of molecular orientation in organic devices. In the field of OLEDs, recent progress has realized an internal electroluminescence quantum efficiency (ϕ_{int}) of nearly 100% even for a nonmetallic compound.[35] Thermally activated delayed fluorescent (TADF) materials[35−43] have a small energy gap between their singlet and triplet excited states that is comparable to the thermal energy at room temperature. As a result, TADF materials can generate singlet excitons by thermal up-conversion from triplet excitons,[39,40] so their OLEDs can show an external electroluminescence quantum efficiency (ϕ_{ext}) as high as those of phosphorescence-based OLEDs. Thus, to further improve ϕ_{ext}, other factors governing ϕ_{ext} now need to be improved; namely, the carrier balance (γ) and out-coupling efficiency (η_{out}). Although η_{out} is difficult to improve by modifying the molecular structure of isolated molecules, molecular configuration can overcome this issue. Specifically, horizontal dipole orientation is advantageous because of the optimal distribution of luminous intensity in the direction normal to the substrate and the suppression of surface plasmon loss; surface plasmons readily couple with vertical dipole oscillations.[12,17−19,41] Accordingly, we investigated the molecular orientational order in thin films fabricated at low $T_{deposition}$ to kinetically control the dynamic behavior of the deposited molecules at the surface. We prepared thin films of 10-[4-(4,6-diphenyl-1,3,5-triazin-2-yl)phenyl]-10*H*-phenoxazine (PXZ-TRZ),[37] which has the simplest linear-shaped structure of reported TADF compounds. To suppress a decrease in γ, a randomly oriented host matrix is also essential according to our previous study.[26] Therefore, we used 3,3-di(9*H*-carbazol-9-yl)biphenyl (mCBP) as a host matrix that has very stable random orientation over a wide range of $T_{deposition}$. In this paper, we demonstrate that the orientational order of PXZ-TRZ can be selectively controlled while maintaining the random orientation of the host matrix, and that ϕ_{ext} can be enhanced by more than 20% because of the improvement in η_{out} associated with the horizontal orientation of PXZ-TRZ.

EXPERIMENTAL SECTION

The structures of the device and compounds used in this study are depicted in Figure 1. Phenoxazine-triphenyltriazine derivative PXZ-TRZ was synthesized as described elsewhere[37] and then sublimed before use. mCBP (Nard Institute Co.),[42,43] *N*,*N*′-diphenyl-*N*,*N*′-di(1-naphthyl)benzidine (α-NPD, Tosoh Organic Chemical Co.), and 1,3,5-tris(*N*-phenylbenzimidazol-2-yl)benzene (TPBi, Jilin OLED Material Tech. Co.) were used as received. Patterned 100 nm thick indium tin oxide (ITO)-coated glass substrates with a sheet resistance of 25 Ω square^{-1} (Atsugi Micro Co.) were carefully cleaned as described elsewhere.[26] Organic layers were formed on the precleaned substrates by vapor deposition at an evaporation rate of 0.1 nm/s under a vacuum of $<1 \times 10^{-3}$ Pa with the sequence: 30 nm thick hole transport layer (α-NPD)/40 nm-thick emitting layer (6 wt % PXZ-TRZ:mCBP)/30 nm-thick electron transport layer (TPBi). $T_{deposition}$ of the emitting layer was varied from 200 to 300 K, whereas $T_{deposition}$ for other layers was kept at 300 K. LiF (0.8 nm)/Al (80 nm) cathodes were vapor deposited on the stack through a shadow mask to form an active area of 4 mm^2. A quartz crystal microbalance (Q-pod, Inficon) was used to monitor the deposition rate of each evaporated material. The fabricated devices were characterized by current density (J)−voltage (V)−luminance (L) and electroluminescence (EL) spectroscopic measurements using an external quantum efficiency (EQE) measurement system (C9920−12, Hamamatsu Photonics) constructed of an integrating sphere with an internal diameter of 3.3 in. optically connected to a calibrated multichannel spectrometer (PMA-12, Hamamatsu Photonics) and a source meter (2400, Keithley) electrically connected to a device placed inside the integrating sphere. Voltage was varied from 0 to 15 V in 0.2 V increments.

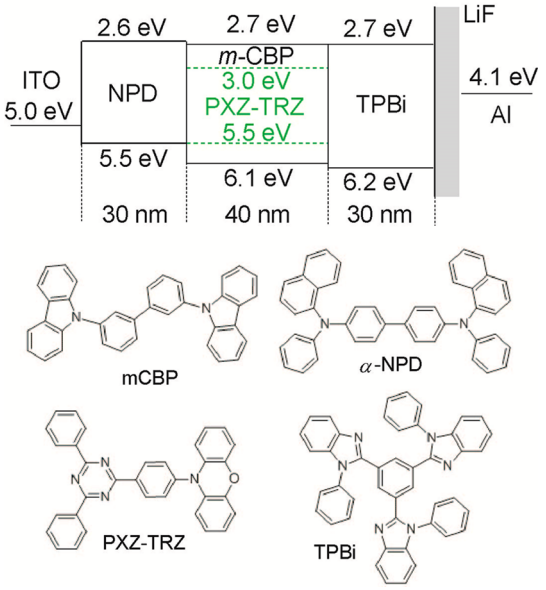

Figure 1. Structure of OLEDs and chemical structures of the compounds used in them.

For photophysical characterization, 40 nm thick 6 wt % PXZ-TRZ:mCBP films were prepared on fused silica substrates by vapor deposition at $T_{deposition}$ = 200, 250, and 300 K. The substrates were carefully cleaned in an identical manner to the ITO substrates. UV−vis spectra were measured on a spectrometer (LAMBDA 950, PerkinElmer) in the range of 250−600 nm with a spectral bandwidth of 1.0 nm. Photoluminescence (PL) spectra excited at 340 nm and PL excitation spectra monitored at 530 nm were measured on a spectrofluorometer (Fluoromax-4, Horiba) in the wavelength ranges of 400−800 and 200−520 nm, respectively. Excitation and emission spectral bandwidths were set to 2.0 nm, and gratings set at 1200 groove/mm blazed at 330 nm (excitation) and 500 nm (emission) were used for the measurements. Photoluminescence quantum efficiencies, ϕ_{PL}, of the films were measured on an absolute PL quantum yield spectrometer (C11347, Hamamatsu Photonics) under an inert atmospheric condition. The obtained spectra were analyzed with specialist software (U6039−05, Hamamatsu Photonics). Samples were excited by a Xe lamp with an excitation wavelength (λ_{ex}) of 330 nm.

The dipole orientation of the dopants was estimated by the dependence of light emission intensity in transverse magnetic (TM) mode on the emission angle (an angular-dependent PL measurement).[41] Films with a thickness of 15 nm were fabricated on glass substrates that were carefully prewashed in the same manner as the fused silica substrates, and were encapsulated with a glass coverslip under an inert atmosphere to avoid photodegradation during the measurement. The samples were then attached to an antireflection-coated half cylinder prism (the refractive index was 1.5) via matching oil, and mounted on a motorized rotation stage (SGSP-120YAW,

dx.doi.org/10.1021/cm500802p | *Chem. Mater.* 2014, 26, 3665−3671

Sigma Koki) with the film surface precisely in the rotational center of the stage. Photoexcitation of the samples (λ_{ex} = 375 nm, <20 mW) was performed using a semiconductor laser light source (DPS-5004, Neoarc) with a band-pass filter (370 ± 5 nm), and measurements were conducted at a fixed incident angle of 45°. The emission from the sample was collected by a calibrated multichannel spectrometer (PMA-11, Hamamatsu Photonics) through a long-pass filter with a cutoff wavelength of 410 nm, a wire-grid-type polarizer (TM mode), and a collimating lens connected to a fiber probe. For precise measurements, the optical axis of the setup was adjusted so that the optical axis of another laser light beam coincided with the center of the rotation stage with an accuracy of <0.5 mm. The radiation patterns were measured automatically, which took less than 10 min for each sample. To evaluate dipole orientation, far-field emission intensity as a function of emission angle was simulated using a commercial software package (setfos 3.4, Fluxim Co.) with an optical model including refractive index (n), extinction coefficient (k), thickness, and dipole orientation p_z/p_x, where substituted z and x indicate the direction of vertical and horizontal to a substrate. Herein, n and k were estimated by variable-angle spectroscopic ellipsometry (VASE) analysis.

To investigate the effect of the estimated dipole orientation on light extraction efficiency, a photonic mode density simulation was conducted using the identical software. Emission spectrum of PXZ-TRZ was modeled in the form of a single dipole source of polarization $P(x, y, z) = (1, 0, 0)$ for the both transverse electric (TE) and transverse magnetic (TM) modes in horizontal dipole or $P(x, y, z) = (0, 0, 1)$ for the TM mode in vertical dipole located at the center of a mCBP layer, and the total power of light coupled out of the devices was estimated by mixing the TE and TM modes considering the dipole ratio p_z/p_x, where the values of p_z/p_x at each $T_{deposition}$ were estimated from the angular-dependent PL measurements. The refractive index of each material was obtained by variable-angle spectroscopic ellipsometry (VASE) analysis.

■ RESULTS AND DISCUSSION

Selectively Controllable Molecular Orientation of Dopants. Molecular shape governs the orientational order in undoped films of vapor-deposited glasses (ordinary and kinetically controlled glasses) prepared at the same substrate temperature. Yokoyama et al.[6,13] pointed out that molecular shape, which determines intermolecular interactions, plays an important role in the formation of orientational order. For example, long linear-shaped molecules are expected to readily adopt a preferential orientation because they do not have substituents around the long axis of the molecule, which would hinder the molecule from lying flat on the substrate through intermolecular interactions. In fact, linear-shaped molecules are reported to exhibit an extremely high orientational parameter $S < -0.45$.[12,13,26] In addition to molecular shape, temperature is the other dominant factor influencing orientational order in vapor-deposited films. Especially at temperatures above T_g, anisotropic molecular orientation becomes easier to reorganize to isotropic via local molecular migration in supercooled liquid states. This is because isotropic orientation in this phase is more thermodynamically stable than anisotropic orientation. In fact, Lin et al.[4,5] reported orientational randomization in spirofluorene-cored noncrystalline films when they were annealed at around or above T_g. Assuming that the molecular shape, T_g, and the temperature of a film define its orientational order, one might consider that molecular orientation can be homogeneously controlled by varying $T_{deposition}$ relative to T_g during deposition. However, noncrystalline films have a depth-dependent distribution of T_g, so $T_{deposition}$ should be varied not against T_g in the bulk material [T_g(bulk)], but against T_g(surface) where the film grows.[24,25] Herein, we define T_g(surface) as the temperature on the border between kinetically and thermodynamically controlled regimes[2] in the resulting molecular packing structure. In a previous study, Yokoyama suggested the possibility that "the T_g at the surface of an organic film is lower than that in the bulk",[6] by considering the experimental observation that orientational orders were randomized even at $T_{deposition}$ much lower than T_g(bulk). Also, we previously demonstrated that orientational randomization initiates at the film surface in thin films of spirofluorene derivatives during thermal annealing.[24] In other words, it is easier for local molecular migration to occur at the surface of a film than in its bulk. In fact, surface diffusion of indomethacin molecules has been reported to be 1×10^6 times faster than their bulk diffusion.[44] Therefore, even though $T_{deposition}$ is lower than T_g(bulk), the kinetic energy of the deposited molecules is expected to be difficult to decrease at the surface when $T_{deposition}$ is higher than T_g(surface), giving rise to local molecular migration (supercooled liquid state) and subsequent orientational randomization (ordinary glass state[45]). The proposed mechanism of molecular orientational randomization is the aggregation induced by weak intermolecular interactions.[9]

To date, control of molecular orientation in noncrystalline films has been achieved for undoped films. However, even in guest−host systems containing a minor fraction of dopant molecules, sufficiently low $T_{deposition}$ might possibly quench the kinetic energy of the deposited molecules, leading to the formation of anisotropic orientation. Accordingly, we investigated the dependence of the molecular orientation of a TADF dopant, PXZ-TRZ, on $T_{deposition}$. Although many TADF compounds adopt winding structures to realize spatial separation of molecular orbitals between the electronic ground and excited states (mainly HOMO and LUMO),[35,36,38−40] PXZ-TRZ forms a linear shape with effective spatial separation between the HOMO and LUMO by having an almost orthogonal dihedral angle of 74.9° between TRZ and PXZ groups.[37] Therefore, we can regard PXZ-TRZ as a linear-shaped molecule because the directions of the transition dipole and molecular long axis are the same. If the molecular orientation (or dipole orientation) of dopants is varied by $T_{deposition}$, a host matrix with random orientation and insensitivity to $T_{deposition}$ should be selected. This is because such a matrix enables us to effectively determine the effect of orientational order of dopants on the electric and optical characteristics of the guest−host system when $T_{deposition}$ is varied. Moreover, random orientation can improve carrier balance in OLEDs because of a small difference between hole and electron mobilities.[26] On the basis of these reasons, we chose mCBP as the host matrix. The molecular orientation of mCBP was investigated by considering optical anisotropy through VASE,[46,47] and the random orientation was fond to be stable at $T_{deposition}$ = 300 K.

A sufficiently high T_1 level is also essential for the host matrix to effectively confine the generated excited energy on TADF dopants. Because the T_1 level of mCBP is 2.8 eV, which is much higher than that of PXZ-TRZ (2.4 eV),[37] the mCBP host is compatible with the PXZ-TRZ dopant. Figure 2a shows the absorption spectra of 40 nm thick 6 wt % PXZ-TRZ:mCBP vapor-deposited films on fused silica substrates. An absorption band appeared at around 340 nm, which mainly originates from the $\pi-\pi^*$ transition of mCBP, and no dependence of $T_{deposition}$ was observed because of the random orientation of mCBP ranging from 200 to 300 K. We attribute the random orientation of mCBP over this wide range of $T_{deposition}$ to its

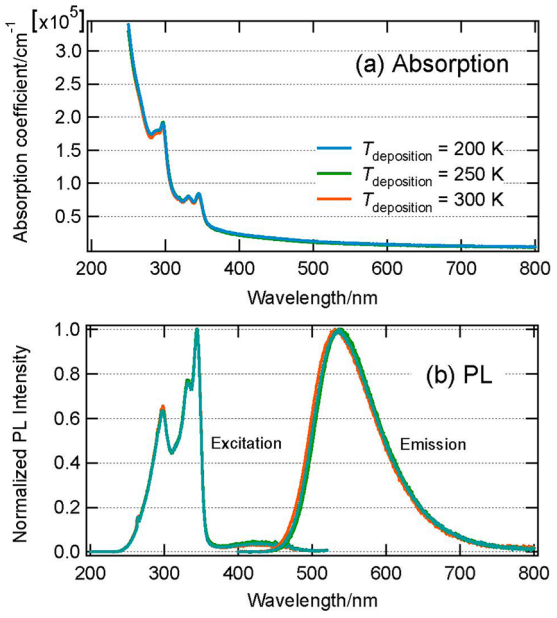

Figure 2. (a) Absorption and (b) PL and excitation spectra obtained for 40 nm-thick 6 wt % PXZ-TRZ:mCBP films prepared on fused silica substrates at $T_{deposition}$ = 200−300 K. An absorption band appeared at around 200 nm, but this band contributes less to generate the emissive excited state, resulting in the difference between the absorption and the PL excitation spectra. The broad excitation band at around 450 nm corresponds to light absorption by PXZ-TRZ, indicating a small Stokes shift.

spherical shape, although T_g(bulk) is relatively high (370 K[42]). When the films were irradiated at 340 nm, excitons photogenerated on mCBP molecules readily donated energy to PXZ-TRZ dopants. Figure 2b shows the PL and excitation spectra of this film. No emission from mCBP was detected, suggesting that effective energy transfer occurred from mCBP to PXZ-TRZ, while bright green emissions from PXZ-TRZ with a peak wavelength of 530 nm were observed. The broad emission spectra originate from the CT character of the PXZ-TRZ molecule consisting of PXZ and TRZ moieties linked by a *p*-phenyl group. The linear-shaped structure of PXZ-TRZ means that the CT transition dipole moment is along the long axis of the molecule, thus allowing us to probe molecular orientational order through CT emission. Molecular orientations in undoped films are often investigated by considering dichroism through polarized optical absorption,[6] but this technique is unsuitable for dopants because of weak absorption intensity and spectral overlap between dopant and matrix. In contrast, Brütting[41] and others[19] used an angular-dependent polarized PL measurement to evaluate dipole orientation. In this technique, emission intensity in a TM mode, which is analogous to *p*-polarization in absorption measurements, is measured at various emission angles. Figure 3a shows the normalized PL intensities as a function of emission angle in 15 nm thick 6 wt % PXZ-TRZ:mCBP films fabricated at $T_{deposition}$ = 200, 250, and 300 K. The angular-dependent PL characteristics clearly show that the relative PL intensity tended to decrease at a large angle as $T_{deposition}$ decreased. Because the vertical dipole emits light preferentially toward the direction lateral to the film surface, this trend of decreasing relative intensity suggests that the distribution of dipole orientation became more horizontal as $T_{deposition}$ decreased. To evaluate this result, the angular-dependent PL characteristics were simulated for various dipole

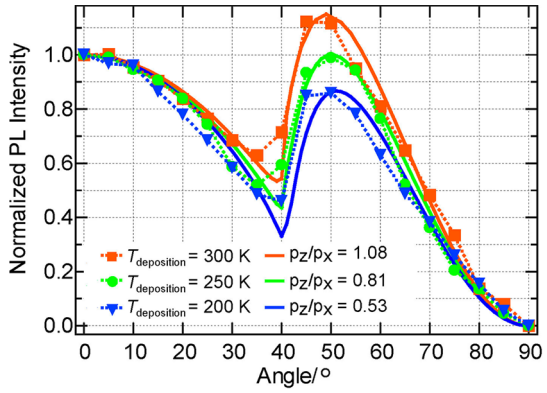

Figure 3. (a) Dependence of light intensity at 530 nm in TM mode on the emission angle in 15 nm thick 6 wt % PXZ-TRZ:mCBP films deposited on glass substrates at $T_{deposition}$ = 200, 250, and 300 K. The estimated values of the dipole ratio (p_z/p_x) are summarized in Table 1

ratios (p_z/p_x). As shown in Figure 3a, the simulations reproduced the experimental results well, and found that the dipole ratio was 0.53, 0.81, and 1.08 at $T_{deposition}$ = 200, 250, and 300 K, respectively. Assuming the same directions of transition dipoles in emission and absorption, the dipole ratio can be transformed into the orientational order parameter S[48,49] by

$$S = \frac{1}{2}\langle 3\cos^2\theta - 1\rangle = \frac{p_z^2 - p_x^2}{p_z^2 + 2p_x^2} \quad (1)$$

where θ is the angle between the normal of a substrate and transition dipole. The calculated S values were −0.31 for $T_{deposition}$ = 200 K, −0.12 for $T_{deposition}$ = 250 K, and 0.05 for $T_{deposition}$ = 300 K. One might suppose that a lower deposition temperature enables the PXZ-TRZ molecules to become more highly oriented. However, mCBP crystallized at temperatures below 100 K. This phenomenon seems strange but is consistent with the report that when $T_{deposition}$ is too low, unstable glasses tend to be generated.[2] Therefore, we limited $T_{deposition}$ to 200−300 K, where the random orientation of mCBP was sufficiently stable.

We ascribe the vertical orientation of PXZ-TRZ at $T_{deposition}$ = 250 and 300 K to partial crystallization or the formation of orientational order via the quasi-equilibrium state where anisotropic orientation coexists with equilibrium properties (e.g., high molar volume).[2] More importantly, as expected, the molecules tended to orient more horizontal to the substrates with decreasing $T_{deposition}$. Lowering $T_{deposition}$ should quench the kinetic energy of the deposited PXZ-TRZ molecules at the film surface, so this result is consistent with our hypothesis that the mechanism of configurational sampling approaches a single-molecule process with decreasing $T_{deposition}$. It is also remarkable that the molecular orientation of PXZ-TRZ was not correlated with that of the mCBP host, indicating that the orientational order of dopants was selectively controllable while maintaining the random orientation of a host matrix. The selective controllability for PXZ-TRZ implies that the migrated mCBP molecules did not completely inhibit the formation process of kinetically controlled preferential orientational order of the PXZ-TRZ molecules, even though mCBP molecules should partially collide with them.

Enhancement of External Electroluminescence Quantum Efficiency. Horizontal dipole orientation of dopants may improve the light out-coupling in OLEDs because of the

dx.doi.org/10.1021/cm500802p | *Chem. Mater.* 2014, 26, 3665−3671

optimal distribution of luminous intensity and suppression of surface plasmon loss.[12,17−19,41] Accordingly, we used the 6 wt % PXZ-TRZ:mCBP guest−host system to enhance ϕ_{ext}. Figure 4

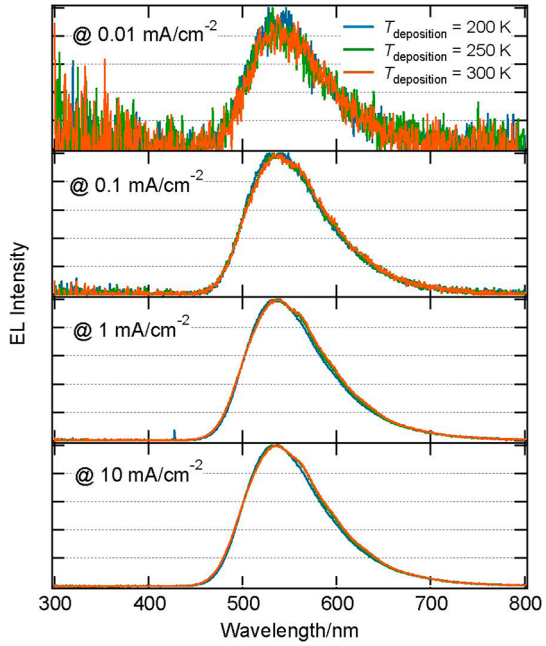

Figure 4. EL spectra measured for OLEDs with the structure shown in Figure 1 and emitting layers deposited at different $T_{deposition}$.

shows the EL spectra of the OLEDs with the device structure shown in Figure 1. No spectral shift was observed in the EL spectra of OLEDs fabricated with different $T_{deposition}$ of the emitting layer. Given that the spatial distribution of excitons affects the spectral shape obtained for similar device structures,[26] this result suggests that the carrier recombination zone did not shift much, and is consistent with the little difference between electron and hole mobilities expected from the isotropic orientation of the host matrix. Because the effect of optical interference, which is correlated with the spatial distribution of excitons, was small, the angular distribution of EL intensity should reflect dipole orientation. Therefore, horizontally oriented dopants in our devices should improve η_{out} to enhance ϕ_{ext}.

Figure 5a shows the ϕ_{ext}−J characteristics of the OLEDs. ϕ_{ext} showed a maximum value of 9.6% at $T_{deposition}$ = 300 K, and became larger with decreasing $T_{deposition}$. At $T_{deposition}$ = 200 K, ϕ_{ext} was 11.9%, which is 24% larger than that at $T_{deposition}$ = 300 K. No crossover of ϕ_{ext} was observed for the devices. Because the three devices differ only in the orientational order of the PXZ-TRZ dopants,[50] this enhancement of ϕ_{ext} is ascribed to the horizontal orientation of PXZ-TRZ at $T_{deposition}$ = 300 K. Interestingly, this dependence of ϕ_{ext} on $T_{deposition}$ was completely opposite to that observed in OLEDs with a light emission layer of 1 wt % 1,2,3,5-tetrakis(carbazol-9-yl)-4,6-dicyanobenzene (4CzIPN):CBP.[26] In contrast to the variation of the molecular orientation of dopant in the PXZ-TRZ:mCBP system, the host matrix possesses variable molecular orientation in the 4CzIPN:CBP system. Again, this contrast leads us to consider that we should bear in mind the use of a host matrix with random orientation and its insensitivity to $T_{deposition}$ if the dipole orientation of a dopant is varied by $T_{deposition}$. To confirm the effect of the molecular orientation of PXZ-TRZ on light

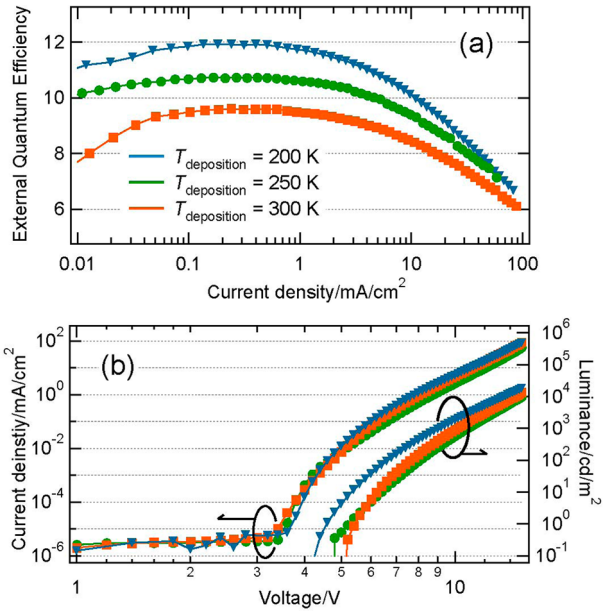

Figure 5. (a) EQE−J and (b) J−V−L characteristics of devices with the structure shown in Figure 1 and emitting layers deposited at different $T_{deposition}$. The maximum values of ϕ_{ext} are summarized in Table 1

out-coupling efficiency, we individually performed photonic mode density simulations using our device structure. A wave-emitting source was placed at the middle of the mCBP layer changing the dipole ratio of p_z/p_x. The dipole ratio p_z/p_x was determined by angular-dependent polarized PL measurements. Note that the far-field emission intensities in horizontal and vertical dipoles ($I_{horizontal}$ and $I_{vertical}$) were obtained by this simulation. The total intensities ($I_{vertical}$ + $2I_{horizontal}$) normalized at $T_{deposition}$ = 300 K are summarized in Table 1, and demonstrate that the total intensity tended to increase with decreasing $T_{deposition}$. The relative intensity at $T_{deposition}$ = 200 K was 1.249, which is comparable to the observed 24% enhancement of ϕ_{ext}. One might consider that the dipole ratios of PXZ-TRZ in OLEDs were deferent from those in angular dependent PL measurements due to the difference in substrates. In fact, dependence of molecular orientation on surface roughness of substrates was reported in the pristine films of 4,4′-bis[(*N*-carbazole)styryl]biphenyl.[51] However, the separately obtained surface roughness values in a glass substrate (angular dependent PL measurements) and α-NPD (OLEDs) were almost the same (0.35−0.4 nm), so we consider that the dipole ratio did not differ in the two measurements.

Because ϕ_{ext} is determined by $\phi_{ext} = \gamma \times \phi_{int} \times \eta_{out}$, the effects of the dependences of γ and ϕ_{int} on $T_{deposition}$ should also be taken into account. Herein, the branching ratios for singlet and triplet excitons are included in ϕ_{int}. Figure 5b shows the J−V−L characteristics obtained for the OLEDs. While L was improved markedly at $T_{deposition}$ = 200 K, the current onset and driving voltage were almost the same for each $T_{deposition}$. Furthermore, EL emissions from carrier transporting layers were not observed at any $T_{deposition}$ (Figure 4). Therefore, the effect of $T_{deposition}$ on γ is expected to be small. This seems consistent with well-balanced γ, supporting the assumption that the carrier recombination zone did not shift much in our OLEDs. This consistency was valid up to at least J = 1 mA/cm^2, although the efficiency roll-off became more substantial above 1 mA/cm^2 as $T_{deposition}$ decreased. The dependence of the

dx.doi.org/10.1021/cm500802p | *Chem. Mater.* 2014, 26, 3665−3671

Table 1. Photophysical and Electroluminescent Properties

	PL						EL	
$T_{deposition}$ (K)	p_z/p_x	S	ϕ_{PL}	τ_{prompt} (ns)	τ_{delay} (μs)	$\Delta E_{S\text{-}T}$ (meV)	ϕ_{ext}	simulated intensity[a]
200	0.53	−0.31	0.736 ± 0.005	16	0.72	32	0.119 ± 0.008	1.249
250	0.81	−0.12	0.723 ± 0.003				0.107 ± 0.003	1.073
300	1.08	0.05	0.694 ± 0.002	16	0.85	36	0.096 ± 0.005	1.000

[a]Normalized at 300 K.

magnitude of the efficiency roll-off on $T_{deposition}$ possibly comes from decreasing ϕ_{int} as $T_{deposition}$ decreased rather than reducing γ because EL from the carrier transporting layers was not observed. Again, the three devices differ only in the orientational order of the PXZ-TRZ dopant, so the horizontal orientation of PXZ-TRZ should cause the efficiency roll-off.

While the effect of γ on ϕ_{ext} was negligible, ϕ_{int} might depend on $T_{deposition}$ even at $J < 1$ mA/cm^2, where the efficiency roll-off did not occur. ϕ_{PL} at each $T_{deposition}$ are summarized in Table 1. The differences of ϕ_{PL} among the films were very small, but ϕ_{PL} increased considerably as $T_{deposition}$ decreased. (ϕ_{PL} at $T_{deposition}$ = 200 K did not change at least for 1 week when we kept the sample under inert atmosphere) However, we believe that this effect was not caused by enhancement of the emission probabilities, but to the difference of intensity of light coupled out of the film. In fact, no difference in the PL and excitation spectra were observed in these films (Figure 2b), suggesting that the electronic structures of PXZ-TRZ in the ground and singlet excited states did not differ between molecules deposited at $T_{deposition}$ = 200 and 300 K. Even in the delayed component, almost the same emission lifetimes were observed: 0.72 μs for $T_{deposition}$ = 200 K and 0.85 μs for $T_{deposition}$ = 300 K. The estimated $\Delta E_{S\text{-}T}$ were 32 meV for $T_{deposition}$ = 200 K and 36 meV for $T_{deposition}$ = 300 K, so the electronic structure of the triplet excited state should not vary either. This is possibly because the environment of the dopants was very stable toward the variation of $T_{deposition}$. The concomitant change of ϕ_{int} arising from microcavity effects[46,52−54] with the variation of the molecular orientation of PXZ-TRZ might possibly affect ϕ_{ext}, but the contribution should be much smaller than that of η_{out} of ∼25%. Thus, we conclude that the horizontal orientation of PXZ-TRZ was the major factor to enhance ϕ_{ext} associated with the improvement of η_{out}, demonstrating the potential use of selective controllability of the molecular orientational order of dopants to optimize OLED performance.

CONCLUSION

The orientational order of the linear-shaped TADF dopant PXZ-TRZ was selectively controlled within a randomly oriented mCBP host matrix at $T_{deposition}$ ranging from 200 to 300 K. When the film was fabricated at 200 K, PXZ-TRZ molecules were oriented horizontal to the substrate, implying that the deposited molecules could reduce the kinetic energy by adopting horizontal orientation in the kinetically controlled regime even in the guest−host system. We attribute this to the molecular interaction between PXZ-TRZ and mCBP being too weak to influence the orientational fluctuation of PXZ-TRZ during the deposition, and consider that the preferential orientation of PXZ-TRZ was intrinsic to the molecular configurations with minimized potential energy.

To demonstrate the potential use of the selective orientation controllability of PXZ-TRZ as an emitting dopant in organic devices, we fabricated EL devices using the 6 wt % PXZ-TRZ:mCBP guest−host system as an emitting layer. With horizontal orientation of dopants, ϕ_{ext} was enhanced by 24%. Horizontally oriented PXZ-TRZ also seemed to facilitate carrier accumulation at the interface(s) with α-NPD and/or TPBi layers, resulting in efficiency roll-off at $J > 1$ mA/cm^2. In addition, a slight optical contribution from a microcavity effect might be included in ϕ_{ext}. This is because radiative decay rate is influenced by electric field at the dipole position, which depends on the dipole orientation of the dopants in a device.[53,54] However, photophysical and electric investigations revealed that the effects of ϕ_{int} and γ were negligible, so we conclude that the enhancement of ϕ_{ext} originates mostly from the horizontal orientation of PXZ-TRZ, which mainly improved η_{out}. Most importantly, this result clearly shows that controlling morphology at the molecular level is worthwhile to maximize the performance of organic devices because even issues limited by the properties of isolated molecules can be overcome.

ASSOCIATED CONTENT

Supporting Information

TD-DFT calculation, extinction coefficient and refractive index spectra, Δ and Ψ spectra, AFM images, dependence of surface roughness on $T_{deposition}$ and T_{anneal}, polarized microscope image, and estimation of $\Delta E_{S\text{-}T}$. This material is available free of charge via the Internet at http://pubs.acs.org.

AUTHOR INFORMATION

Corresponding Author

*E-mail: adachi@cstf.kyushu-u.ac.jp.

Notes

The authors declare no competing financial interest.

ACKNOWLEDGMENTS

This work was supported in part by the Funding Program for World-Leading Innovative R&D on Science and Technology (FIRST) and the International Institute for Carbon Neutral Energy Research (WPI-I2CNER) sponsored by the Ministry of Education, Culture, Sports, Science and Technology (MEXT). T. K. thanks Hiroko Nomura for helping to purify PXZ-TRZ and Christian Mayr for his contribution of estimating the dipole orientation (PXZ-TRZ at 300 K).

REFERENCES

(1) Forrest, S. R. *Chem. Rev.* **1997**, *97*, 1793.
(2) Dalal, S. S.; Fakhraai, Z.; Ediger, M. D. *J. Phys. Chem. B* **2013**, *117*, 15415.
(3) Lin, H. W.; Lin, C. L.; Chang, H. H.; Lin, Y. T.; Wu, C. C.; Chen, Y. M.; Chen, R. T.; Chien, Y. Y.; Wong, K. T. *J. Appl. Phys.* **2004**, *95*, 881.
(4) Lin, H. W.; Lin, C. L.; Wu, C. C.; Chao, T. C.; Wong, K. T. *Org. Electron.* **2007**, *8*, 189.
(5) Cheng, H. C.; Lin, H. W.; Wu, C. C.; Wong, K. T.; Kuan, C. H. *Proc. SPIE* **2007**, *6655*, 66551X.
(6) Yokoyama, D. *J. Mater. Chem.* **2011**, *21*, 19187.

(7) Yokoyama, D.; Sasabe, H.; Furukawa, Y.; Adachi, C.; Kido, J. *Adv. Funct. Mater.* **2011**, *21*, 1375.
(8) Yokoyama, D.; Park, Y.; Kim, B.; Kim, S.; Pu, Y. J.; Kido, J.; Park, J. *Appl. Phys. Lett.* **2011**, *99*, 123303.
(9) Yokoyama, D.; Setoguchi, Y.; Sakaguchi, A.; Suzuki, M.; Adachi, C. *Adv. Funct. Mater.* **2010**, *20*, 386.
(10) Yokoyama, D.; Sakaguchi, A.; Suzuki, M.; Adachi, C. *Appl. Phys. Lett.* **2009**, *95*, 243303.
(11) Yokoyama, D.; Adachi, C. *J. Appl. Phys.* **2010**, *107*, 123512.
(12) Frisheisen, J.; Yokoyama, D.; Adachi, C.; Brütting, W. *Appl. Phys. Lett.* **2010**, *96*, 073302.
(13) Yokoyama, D.; Sakaguchi, A.; Suzuki, M.; Adachi, C. *Org. Electron.* **2009**, *10*, 127.
(14) Yokoyama, D.; Sakaguchi, A.; Suzuki, M.; Adachi, C. *Appl. Phys. Lett.* **2008**, *93*, 173302.
(15) Kim, J. Y.; Yokoyama, D.; Adachi, C. *J. Phys. Chem. C* **2012**, *116*, 8699.
(16) Komino, T.; Nomura, H.; Endo, K.; Yahiro, M.; Adachi, C. *J. Phys. Chem. C* **2011**, *115*, 19890.
(17) Taneda, M.; Yasuda, T.; Adachi, C. *Appl. Phys. Express* **2011**, *4*, 071602.
(18) Frisheisen, J.; Yokoyama, D.; Endo, A.; Adachi, C.; Brütting, W. *Org. Electron.* **2011**, *12*, 809.
(19) Flämmich, M.; Frischeisen, J.; Setz, D. S.; Michaelis, D.; Krummacher, B. C.; Schmidt, T. D.; Brütting, W.; Danz, N. *Org. Electron.* **2011**, *12*, 1663.
(20) Egelhaaf, H.-J.; Gierschner, J.; Haiber, J.; Oelkrug, D. *Opt. Mater.* **1999**, *12*, 395.
(21) Oelkrug, D.; Egelhaaf, H.-J.; Haiber, J. *Thin Solid Films* **1996**, *284*−*285*, 267−270.
(22) Oh-e, M.; Ogata, H.; Fujita, Y.; Koden, M. *Appl. Phys. Lett.* **2013**, *102*, 101905.
(23) Schuenemann, C.; Petrich, A.; Schulze, R.; Wynands, D.; Meiss, J.; Hein, M. P.; Jankowski, J.; Elschner, C.; Alex, J.; Hummert, M.; Eichhorn, K. J.; Leo, K.; Riede, M. *Org. electron.* **2013**, *14*, 1704.
(24) Komino, T.; Nomura, H.; Yahiro, M.; Adachi, C. *J. Phys. Chem. C* **2012**, *116*, 11584.
(25) Komino, T.; Nomura, H.; Yahiro, M.; Adachi, C. *Chem. Phys. Lett.* **2013**, *563*, 70.
(26) Komino, T.; Nomura, H.; Koyanagi, T.; Adachi, C. *Chem. Mater.* **2013**, *25*, 3038.
(27) Keddie, J. L.; Jones, R. A. L.; Cory, R. A. *Europhys. Lett.* **1994**, *27*, 59.
(28) Keddie, J. L.; Jones, R. A. L.; Cory, R. A. *Faraday Discuss.* **1994**, *98*, 219.
(29) Kim, C.; Facchetti, A.; Marks, T. J. *Science* **2007**, *318*, 76.
(30) Kim, C.; Facchetti, A.; Marks, T. J. *J. Am. Chem. Soc.* **2009**, *131*, 9122.
(31) Bakken, N.; Torres, J. M.; Li, J.; Vogt, B. D. *Soft Matter.* **2011**, *7*, 7269.
(32) Torres, J.; Bakken, N.; Stafford, C. M.; Li, J.; Vogt, B. D. *Soft Matter.* **2010**, *6*, 5783.
(33) Noguchi, Y.; Sato, N.; Tanaka, Y.; Nakayama, Y.; Ishii, H. *Appl. Phys. Lett.* **2008**, *92*, 203306.
(34) Noguchi, Y.; Miyazaki, Y.; Tanaka, Y.; Sato, N.; Nakayama, Y.; Schmidt, T. D.; Brütting, W.; Ishii, H. *J. Appl. Phys.* **2012**, *111*, 114508.
(35) Uoyama, H.; Goushi, K.; Shizu, K.; Nomura, H.; Adachi, C. *Nature* **2012**, *492*, 234.
(36) Zhang, Q.; Lie, J.; Shizu, K.; Huang, S.; Hirata, S.; Miyazaki, H.; Adachi, C. *J. Am. Chem. Soc.* **2012**, *134*, 14076.
(37) Tanaka, H.; Shizu, K.; Miyazaki, H.; Adachi, C. *Chem. Commun.* **2012**, *48*, 11394.
(38) Sato, K.; Shizu, K.; Yoshimura, K.; Kawada, A.; Miyazaki, H.; Adachi, C. *Phys. Rev. Lett.* **2013**, *110*, 247401.
(39) Endo, A.; Sato, K.; Yoshimura, K.; Kai, T.; Kawada, A.; Miyazaki, H.; Adachi, C. *Appl. Phys. Lett.* **2011**, *98*, 083302.
(40) Endo, A.; Ogasawara, M.; Takahashi, A.; Yokoyama, D.; Kato, Y.; Adachi, C. *Adv. Mater.* **2009**, *21*, 4802.
(41) Brütting, W.; Frischeisen, J.; Schmidt, T. D.; Scholz, B. J.; Mayr, C. *Phys. Status Solidi A* **2013**, *210*, 44.
(42) Schrögel, P.; Langer, N.; Schildknecht, C.; Wagenblast, G.; Lennartz, C.; Strohriegl, P. *Org. Electron.* **2011**, *12*, 2047.
(43) Gong, S.; He, X.; Chen, Y.; Jiang, Z.; Zhong, C.; Ma, D.; Qin, J.; Yang, C. *J. Mater. Chem.* **2012**, *22*, 2894.
(44) Zhu, L.; Brian, C. W.; Swallen, S. F.; Straus, P. T.; Ediger, M. D.; Yu, L. *Phys. Rev. Lett.* **2011**, *106*, 526103.
(45) Quasi equilibrium state might possibly also be generated in the temperature regime $T_g(\text{surface}) < T_{\text{deposition}} < T_g(\text{bulk})$. However, we could not differentiate the quasi equilibrium state from equilibrium state, so we include this temperature regime in the equilibrium state in this study.
(46) Fujiwara, H. *Spectroscopic Ellipsometry: Principles and Applications*; Wiley: New York, 2007.
(47) Woolam, J. A.; Johs, B.; Herzinger, C. M.; Hilfiker, J.; Synowicki, R.; Bungay, C. L. *Proc. SPIE* **1999**, *CR72*, 3.
(48) Graf, H. M.; Zobel, O.; East, A. J.; Haarer, D. *J. Appl. Phys.* **1995**, *75*, 3335.
(49) Cao, X.; McHale, J. L. *J. Phys. Chem. B* **1997**, *101*, 8843.
(50) Molecular orientation of α-NPD did not change. In fact, molecular orientation in stacked undoped films has already been investigated thoroughly by in situ spectroscopic ellipsometry.[11]
(51) Yokoyama, D.; Setoguchi, Y.; Sakaguchi, A.; Suzuki, M.; Adachi, C. *Adv. Funct. Mater.* **2010**, *20*, 386.
(52) Krummacher, B. C.; Nowy, S.; Frischeisen, J.; Klein, M.; Brütting, W. *Org. Electron.* **2009**, *10*, 478.
(53) Nowy, S.; Krummacher, B. C.; Frischeisen, J.; Reinke, N. A.; Brütting, W. *J. Appl. Phys.* **2008**, *104*, 123109.
(54) Becker, H.; Burns, S. E.; Friend, R. H. *Phys. Rev. B* **1997**, *56*, 1893.